High-Accuracy Point Positioning with Low-Cost GPS Receivers: How Good Can It Get?

Tomas Beran[1], Richard B. Langley[1], Sunil B. Bisnath[2] and Luis Serrano[1]

[1] *Geodetic Research Laboratory, Department of Geodesy and Geomatics Engineering*
University of New Brunswick, Fredericton, New Brunswick, Canada
[2] *Harvard-Smithsonian Center for Astrophysics, Cambridge, Massachusetts, U.S.A.*

BIOGRAPHIES

Tomas Beran received his Master's degree in surveying science from the Czech Technical University in Prague in 1999. He is currently a Ph.D. candidate in the Department of Geodesy and Geomatics Engineering at the University of New Brunswick (UNB), where he is investigating the use of GPS for single-frequency precise point positioning. His research is being performed under the supervision of Professor Richard Langley in the department's Geodetic Research Laboratory.

Richard Langley is a professor in the Department of Geodesy and Geomatics Engineering at the University of New Brunswick, where he has been teaching and conducting research since 1981. He has a B.Sc. in applied physics from the University of Waterloo and a Ph.D. in experimental space science from York University, Toronto. Professor Langley has been active in the development of GPS error models since the early 1980s and is a contributing editor and columnist for GPS World magazine. He is a fellow of the Institute of Navigation (ION) and shared the ION Burka Award for 2003.

Sunil Bisnath is a geodesist at the Harvard-Smithsonian Center for Astrophysics in Cambridge, Massachusetts, where his responsibilities include management of the Basin and Range Geodetic Network (BARGEN). Previously, Dr. Bisnath worked as a GPS research scientist in the Hydrographic Science Research Center at the University of Southern Mississippi. He received an Honours B.Sc. and a M.Sc. in surveying science from the University of Toronto and a Ph.D. from the University of New Brunswick.

Luis Serrano obtained his Diploma in geographic engineering from the Faculty of Sciences of the University of Lisbon in 2000. During the following 4 years he worked in the geodetic engineering profession. Currently he is a Ph.D. student in the Department of Geodesy and Geomatics Engineering at the University of New Brunswick, where he carries out research in precise navigation.

ABSTRACT

High-accuracy, point positioning has been an attractive research topic in the GPS community for a number of years. The overall quality of precise point positioning results is also dependent on the quality of the GPS measurements and user's processing software. Dual-frequency, geodetic-quality GPS receivers are routinely used both in static and kinematic applications for high-accuracy point positioning. However, use of low-cost, single-frequency GPS receivers in similar applications creates a challenge because of how the ionosphere, multipath and other measurement error sources are handled. In this paper, we examine the potential use of such receivers to provide horizontal positioning accuracies of a few decimetres. Practical applications of post-processed, high-accuracy, single-frequency point positioning include a myriad of terrestrial and space-borne applications, where the size and cost of the GPS unit is an issue.

Our processing technique uses pseudorange and time-differenced carrier-phase measurements in a sequential least-squares filter. In developing our approach, we have attempted to separate and examine each measurement error, describe its properties and maximum error effect on the results, and implement algorithms to mitigate it. Ionospheric delay grid maps are used to remove the bulk of the ionospheric error, while tropospheric error is handled by a prediction model. Pseudorange multipath errors are mitigated by means of stochastic modelling and

carrier-phase cycle slips are detected and corrupted measurements are removed in a quality-control algorithm.

The technique was first tested on L1 measurements extracted from static datasets from static, high-quality GPS receivers. Accuracies better than two-decimetres in horizontal components (northing and easting r.m.s.), and three-decimetre accuracies in the vertical component (up-component r.m.s.), were obtained. A test dataset from a stationary low-cost GPS receiver has been processed to demonstrate the difference in data quality. Positioning results obtained are worse than those of a high-quality GPS receiver, but they are still within the few decimetre (dm) accuracy level (northing and easting r.m.s.). The use of the technique is not restricted to static applications, and the results of kinematic experiments are also presented.

INTRODUCTION

In order to achieve high-accuracy point positioning results using GPS, numerous research groups have used dual-frequency, geodetic-quality receiver data. The UNB Geodetic Research Laboratory (GRL) achieved sub-dm-level results in this research area [Bisnath, 2004]. The Geodetic Survey Division of Natural Resources Canada introduced an on-line precise positioning service that facilitates access to the Canadian Spatial Reference Frame (CSRS-PPP). The providers of the service claim that the resulting accuracy is comparable to phase-differential GPS, for dual and single-frequency geodetic-quality receiver data [Tétreault et al., 2005]. Researchers from the Jet Propulsion Laboratory (JPL) [Muellerschoen et al., 2004] evaluated the real-time positioning performance of a single-frequency receiver using the 1-Hz differential corrections provided by NASA's Global Differential GPS System. The results obtained using single-frequency data from a geodetic-quality receiver are of similar accuracy to those obtained by the CSRS-PPP. We are presently investigating the possibility of using *low-cost*, single-frequency GPS receivers for high-accuracy precise point positioning.

The choice of the functional model used in this paper is based on previous research. Four functional models were investigated by Beran et al. [2004]: 1) the pseudorange-only position model – the basic navigation solution, 2) the pseudorange model with between-satellite differences, which removes the receiver clock error, 3) the pseudorange model in the sequential least-squares solution, taking into account all previous estimates, and 4) the pseudorange and time-differenced carrier-phase model, which operates in a fashion similar to model #3, but also takes position-changes between epochs into account. Previously, Beran et al. [2003] investigated two types of Kalman filter-based functional models: 5) the pseudorange and carrier-phase model which is more

suitable for static positioning applications and 6) the pseudorange and time-differenced carrier-phase model which is suitable for platforms with near-constant accelerations. For models #5 and #6, some a priori knowledge of the platform dynamics is required.

It was concluded that the pseudorange and time-differenced carrier-phase model #4 is the most suitable for general purpose, high-precision point-positioning applications, because it does not require any a priori knowledge of platform dynamics, instead of this the dynamic information is obtained directly from the time-differenced carrier-phase measurements.

FILTER MODEL

The pseudorange and time-differenced carrier-phase model is presented here to show the fusion of pseudorange data with the factor-100-more-precise time-differenced carrier-phase data. Time-differenced carrier-phase data also provide a connection between measurement epochs, so the actual velocity measurements (time-differenced carrier phases) provide the dynamic information to the filter [Bisnath and Langley, 2002].

The linearized pseudorange and time-differenced carrier-phase filter observation model in hypermatrix form is

$$\begin{bmatrix} \mathbf{P}_t - \mathbf{P}_t^0 \\ \delta\boldsymbol{\Phi}_{t,t-1} - \delta\boldsymbol{\Phi}_{t,t-1}^0 \end{bmatrix} = \begin{bmatrix} 0 & \mathbf{A}_t \\ -\mathbf{A}_{t-1} & \mathbf{A}_t \end{bmatrix} \begin{bmatrix} \delta\mathbf{x}_{t-1} \\ \delta\mathbf{x}_t \end{bmatrix} + \begin{bmatrix} \mathbf{e}_t \\ \boldsymbol{\varepsilon}_{t,t-1} \end{bmatrix};$$
$$\mathbf{C}_{\mathbf{P}_t}, \ \mathbf{C}_{\delta\boldsymbol{\Phi}_{t,t-1}},$$

(1)

where $\mathbf{P}_t$ and $\mathbf{P}_t^0$ are the pseudorange measurement and predicted value, respectively; $\delta\boldsymbol{\Phi}_{t,t-1}$ and $\delta\boldsymbol{\Phi}_{t,t-1}^0$ are the time-differenced carrier phase measurement and predicted value, respectively; $\delta\mathbf{x}_{t-1}$ and $\delta\mathbf{x}_t$ are the estimated corrections to the receiver position and clock at epochs t-1 and t, respectively; $\mathbf{A}_{t-1}$ and $\mathbf{A}_t$ are the measurement design matrices for epochs t-1 and t, respectively; $\mathbf{e}_t$ and $\boldsymbol{\varepsilon}_{t,t-1}$ are the measurement errors associated with $\mathbf{P}_t$ and $\delta\boldsymbol{\Phi}_t$, respectively; $\mathbf{C}_{\mathbf{P}_t}$ and $\mathbf{C}_{\delta\boldsymbol{\Phi}_{t,t-1}}$ are the covariance matrices for $\mathbf{P}_t$ and $\delta\boldsymbol{\Phi}_{t,t-1}$, respectively. Note that at present in the model the pseudorange and carrier-phase measurements are assumed uncorrelated between observables and between observations.

The best solution for (1), in a least-squares sense, is

$$
\begin{bmatrix} \hat{\mathbf{x}}_{t-1} \\ \hat{\mathbf{x}}_t \end{bmatrix}
$$

$$
= \begin{bmatrix} \mathbf{x}_{t-1}^0 \\ \mathbf{x}_t^0 \end{bmatrix} - \begin{bmatrix} \mathbf{A}_{t-1}^T \mathbf{C}_{\delta\Phi_{t,t-1}}^{-1} \mathbf{A}_{t-1} + \mathbf{C}_{\hat{\mathbf{x}}_{t-1}}^{-1} & -\mathbf{A}_{t-1}^T \mathbf{C}_{\delta\Phi_{t,t-1}}^{-1} \mathbf{A}_t \\ -\mathbf{A}_t^T \mathbf{C}_{\delta\Phi_{t,t-1}}^{-1} \mathbf{A}_{t-1} & \mathbf{A}_t^T \left(\mathbf{C}_{\mathbf{p}_t}^{-1} + \mathbf{C}_{\delta\Phi_{t,t-1}}^{-1} \right) \mathbf{A}_t \end{bmatrix}^{-1}
$$

$$
\times \begin{bmatrix} -\mathbf{A}_{t-1}^T \mathbf{C}_{\delta\Phi_{t,t-1}}^{-1} \mathbf{w}_{\delta\Phi} \\ \mathbf{A}_t^T \mathbf{C}_{\mathbf{P}_t}^{-1} \mathbf{w}_{\mathbf{P}} + \mathbf{A}_t \mathbf{C}_{\delta\Phi_{t,t-1}}^{-1} \mathbf{w}_{\delta\Phi} \end{bmatrix},
$$

(2)

where $\mathbf{w}_\mathbf{P}$ and $\mathbf{w}_{\delta\Phi}$ are the misclosure vectors for the pseudoranges and time-differenced carrier phases, respectively; and $\mathbf{C}_{\hat{\mathbf{x}}_{t-1}}$ is the receiver-estimated position and clock covariance matrix based on the last epoch's solution.

Point positioning processing modelling considerations include relativistic GPS satellite clock correction due to the eccentricity of GPS satellite orbits; GPS satellite antenna phase centre to centre-of-mass offset; GPS satellite phase wind-up due to the relative rotation of the GPS satellite antennas with respect to a receiver antenna; sub-diurnal variations in Earth rotation; solid Earth tides; ocean tide loading; and consistency between models used in the generation of GPS orbits and clocks and models used in the point positioning processing [Kouba and Héroux, 2001]. Our processor currently includes all point positioning processing modelling considerations except the solid Earth tides and ocean tide loading, satellite phase wind-up and sub-diurnal variations in Earth rotation.

Atmospheric effects should also be considered in order to obtain precise and accurate point positioning results. These effects include the ionospheric delay and the tropospheric delay.

Ionosphere – Even though there is a measurement linear combination available to minimize the effect of the ionosphere, [e.g., Muellerschoen et al., 2004], external corrections from IGS ionospheric products (rapid and final) could be also applied. The slant ionospheric delays are computed from the geographic grid of total electron content (TEC) values or the ionosphere maps generated by some IGS processing centres [Schaer et al. 1998]. IGS rapid and final ionospheric grid maps were used in our tests.

Troposphere – The UNB3 tropospheric delay prediction model, which we have used in our analyses, consists of the Saastamoinen zenith tropospheric model, Niell mapping functions, a surface met lookup table and height propagators [Collins, 1999].

Discontinuities in the carrier-phase observations usually referred to as cycle slips, and the negative influence of multipath should be handled in the processing model.

Cycle slips – The loss of carrier-phase tracking resulting in an integer number of cycles discontinuity will cause an error in the carrier-phase measurements. A residual outlier detection algorithm runs separately on both pseudorange and delta carrier-phase observations. If an outlier is detected, the corresponding satellite is removed and a new solution is generated and tested. If too many delta carrier-phase measurements are rejected, the processor generates a code-only solution and the filter is reset.

Multipath – Typical multipath error in the pseudorange measurement varies from about 1 m to 5 m. Multipath in the pseudorange measurements are usually two orders of magnitude bigger than the multipath errors in the carrier-phase measurements [Misra and Enge, 2001]. Pseudorange multipath errors will have an impact mostly on low-elevation angle measurements, so one of the processor configuration settings is elevation angle cut-off.

DATA TESTING AND ANALYSIS

Static and kinematic tests were performed to demonstrate the capabilities of the single-frequency point-positioning technique. In all cases IGS final ephemerides and GPS satellite high-rate clock information were used. For the static tests the IGS final ionospheric grid maps were used and for the kinematic test the IGS rapid ionospheric grid maps were used.

Static Data Testing

The purpose of the first static test was to compare the results from high-quality (Algonquin IGS station, Algonquin Park, Canada) and low-quality (UNB Gillin Hall control monument) GPS data covering the same period of time on 22 February 2005. The Algonquin IGS station (ALGO) is equipped with an AOA BenchMark ACT GPS receiver with the AOA D/M_T choke-ring antenna and a hydrogen maser clock. Only single-frequency, 30 s, measurements were used in the Algonquin data processing. A Garmin GPS 12XL handheld receiver with Garmin GA27C low profile remote automobile antenna was placed on the UNB Gillin Hall control monument. Garmin data logging software including a Garmin RINEX converter developed by Prof. Antonio Taberrano from the Computer Science School, Technical University of Madrid was used. It is available on his Web site (http://artico.lma.fi.upm.es/numerico/miembros/antonio/async/). UNB Gillin Hall GPS data were downsampled from 1 s to 30 s (see Table 6 for more information on the choice of the sampling rate). A 15-

degree elevation angle cut-off was applied to both datasets.

The results of the Algonquin IGS station processing are presented in Figures 1 and 2. The north, east and up component error values were computed by subtracting the reference IGS coordinates from the estimated position. After 20 epochs of data position estimates achieved about 1 dm standard deviations in horizontal error components and 2 dm in the vertical component respectively (Table 1). Less than 2 dm up component bias is probably caused by residual atmospheric errors.
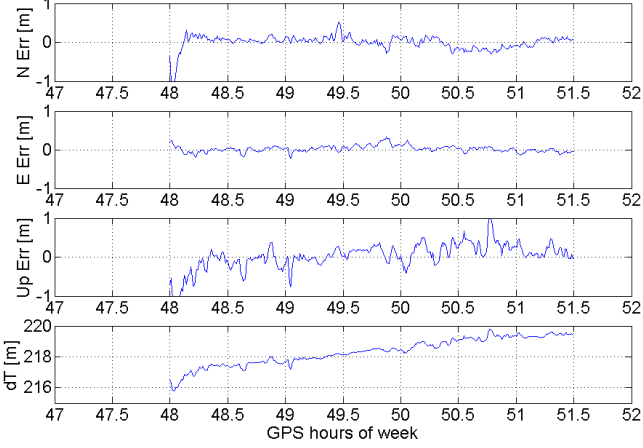
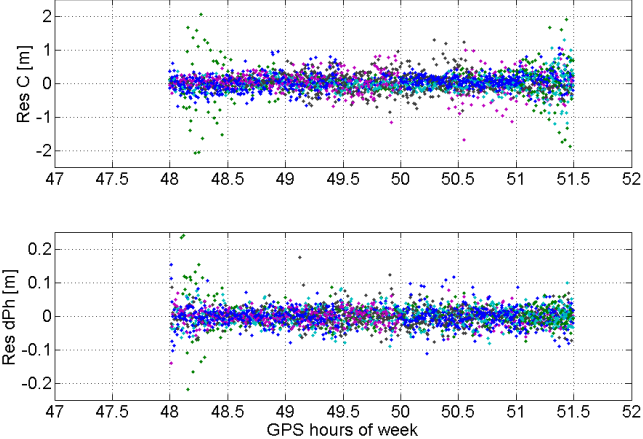Figure 1: Position component and receiver clock errors of the Algonquin IGS station L1 data processing.

Figure 2: Filter residuals from Algonquin IGS station L1 data processing. Top: pseudoranges. Bottom: carrier-phase differences.

Position Error Components [cm]			
	North	East	Up
Mean	2.0	2.0	7.0
Std. Dev.	13.0	8.0	26.0
r.m.s.	13.0	8.0	27.0
Measurement Residual r.m.s. [cm]			
Code	30.0	dPhase	3.0

Table 1: Algonquin data processing statistics ignoring the initial 20 epochs of data.

The results of the Gillin Hall data processing are presented in Figures 3 and 4. The more than 2 m errors from the first 30 minutes of data reflect a code-only solution, selected by the filter because of the discontinuities in the initial carrier-phase data. Low-quality observations also cause problems in the north-component error near hour 50.5. Reference coordinates of the Gillin Hall monument were obtained from the New Brunswick survey control network database.
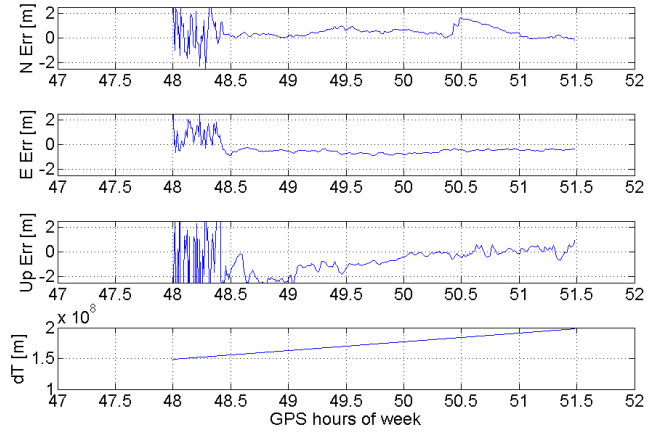

Figure 3: Position component and receiver clock errors of the UNB Gillin Hall station data processing. Please note the different scales when comparing with Figure 1.
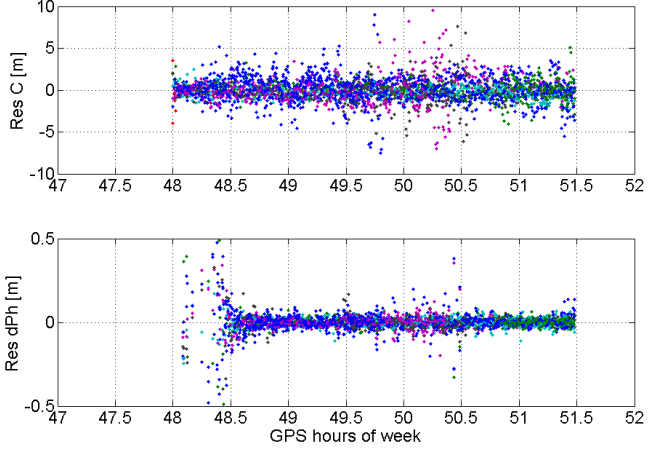

Figure 4: Filter residuals from UNB Gillin Hall station L1 data processing. Top: pseudoranges. Bottom: carrier-phase differences. Please note the different scales when comparing with Figure 2.

Position Error Components [cm]			
	North	East	Up
Mean	47.0	-54.0	-69.0
Std. Dev.	39.0	14.0	85.0
r.m.s.	61.0	56.0	110.0
Measurement Residual r.m.s. [cm]			
Code	157.0	dPhase	6.0

Table 2: Gillin Hall data processing statistics ignoring the initial 60 epochs of data.

Table 2 shows the statistics of the results from the epoch 61 to the end of the dataset. The 60-epoch time period was selected to remove the initial period of time with code-only solution from the statistics. There are a few-dm level biases in all position components and few-dm level standard deviations for the north and up position components. Code measurement residuals (top part of Figure 4) and the code measurement residual statistics (Table 2) indicate problems with the measurement quality.

Previous investigations [Boudreau, 1993] and further analysis (see Figure 16) show that the UNB Gillin Hall site is a high-multipath environment. Since the Gillin Hall dataset represents a bad scenario, we also processed Garmin receiver data from the roof of Head Hall at UNB (the code residual r.m.s. values are about half of those of Gillin Hall) from 20 June 2005. These data were also processed with the same processing parameters as those used for the Gillin Hall station. The results of the Head Hall data processing are presented in Figure 5 and Figure 6 and Table 3. Reference coordinates of the Head Hall station were obtained from a commercial GPS software Gillin Hall – Head Hall baseline solution using 2 hours of Trimble 5700 receiver data.
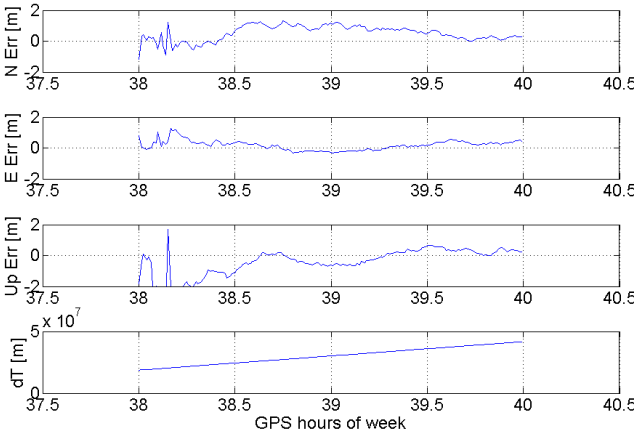

Figure 5: Position component and receiver clock errors of the UNB Head Hall station data processing.
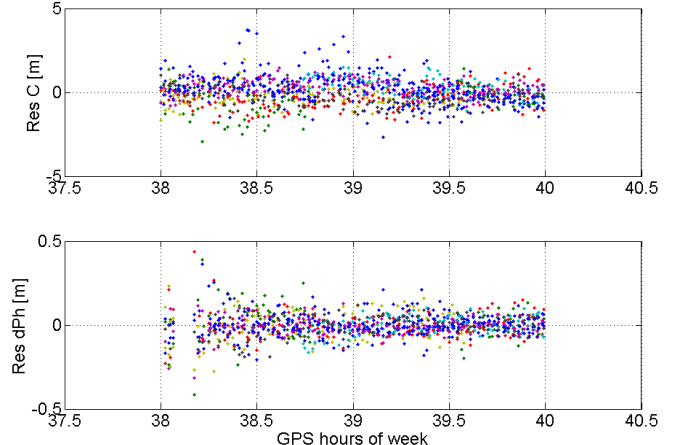

Figure 6: Filter residuals from UNB Head Hall data processing. Top: pseudoranges. Bottom: carrier-phase differences.

Position Error Components [cm]			
	North	East	Up
Mean	39.0	0.0	-23.0
Std. Dev.	13.0	4.0	7.0
r.m.s.	41.0	4.0	24.0
Measurement Residual r.m.s. [cm]			
Code	81.0	dPhase	7.0

Table 3: Head Hall data processing statistics for the 39-40 hour time period ignoring the initial 30 epochs of data.

The position error component statistics (Table3) show approximately 4 dm r.m.s. or less in all components after 30 epochs. The initial 30-epoch time period was ignored due to the code-only solution in computing the statistics. The north component bias remains to be investigated. Delta phase residuals in Figure 6 indicate ~1 metre peak-to-peak variations around hour 38.4 caused by a filter reset to a code-only solution for some minutes.

Kinematic Data Testing

Kinematic data were collected on 4 August 2005. A Trimble 5700 dual-frequency, geodetic-quality GPS receiver with a Zephyr antenna and a Garmin GPS 12XL handheld receiver with a Garmin GA27C low profile remote automobile antenna were mounted on the roof of a car. The car was driven on two and four-lane highways and residential areas of Fredericton, New Brunswick, Canada for about 2 hours (see Figure 7).
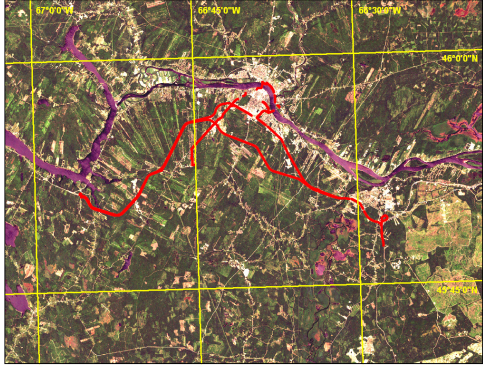
Figure 7: Test trajectory (red) on a Landsat satellite image of a 20 x 20 km area surrounding the city of Fredericton, New Brunswick, Canada.

The reference solution for the Trimble antenna position was a kinematic baseline solution obtained with commercial GPS processing software with a static reference station at UNB Gillin Hall. An approximately 15-minute period of data with a reliable ambiguity-fixed solution was selected.
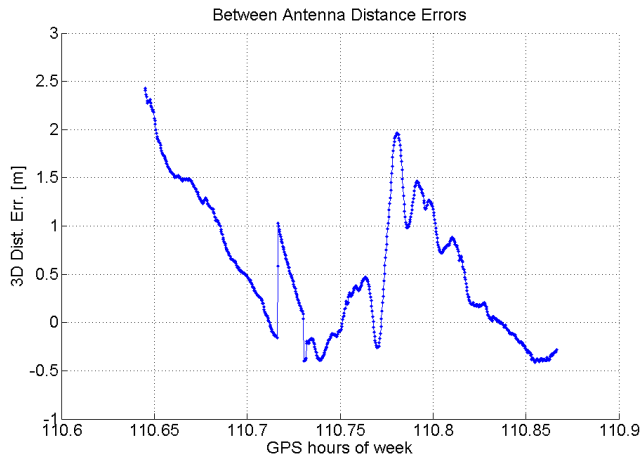

Figure 8: Estimated 3D distance error between the Garmin and Trimble antennas.

Even though a short period of data with good GPS signal reception was selected from the Garmin 2-hour dataset, the peak-to-peak variations in the position component differences reach almost the 4-metre level. The low quality of the Garmin data solution is further demonstrated by the plots of code and delta-phase residuals in Figure 9.
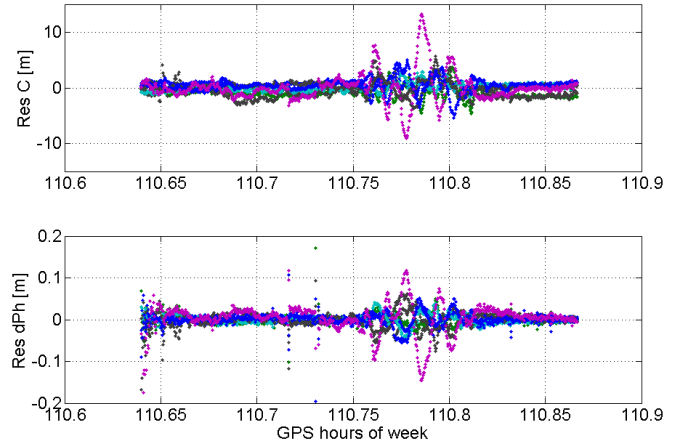

Figure 9: Filter residuals from of the Garmin data processing of data collected during the kinematic experiment. Top: pseudoranges. Bottom: carrier-phase differences.

Filter residuals in Figure 9 shows large variations in code and delta-phase residuals between hours 110.75 and 110.8 as well as individual delta-phase outliers between hours 110.7 and 110.75. These problematic periods correspond to metre-level variations and discontinuities in the position component differences and are most likely caused by undetected measurement outliers in the measurements.

Position Error Components [cm]			
	North	East	Up
Mean	86.0	-4.0	-69.0
Std. Dev.	56.0	35.0	123.0
r.m.s.	103.0	35.0	141.0
Measurement Residual r.m.s. [cm]			
Code	151.0	dPhase	2.0

Table 4: Garmin kinematic data processing statistics ignoring the initial 20 epochs of data. Note: Statistics include 57 cm bias (see below).

Table 4 shows the statistics of position component differences between the Trimble antenna coordinates (relative carrier-phase solution) and Garmin antenna coordinates (point positioning solution). The north and east position components statistics are absorbing most of the between antenna distance (see below), but we do not expect to see large variations in the up component difference. More than metre-level standard deviation in the up component and about 1.5 m r.m.s. of the code residuals indicate problems in the Garmin data quality (see more details in the Discussion section).

The distance between the two antennas mounted on the car is 57 cm. The statistics of 3D between-antenna distance, computed from the position component differences, are: mean of 98 cm, std. dev. of 58 cm.

Figure 8 shows the error in the distance computed from the Trimble antenna coordinates and the Garmin antenna coordinates.

The single-frequency observations from the Trimble dataset were also processed by the point positioning filter. The direct comparison of the point positioning solution and the reference relative carrier-phase solution displayed in Figure 10 shows good agreement. Decimetre-level r.m.s. of the position component differences were obtained in both horizontal and vertical components. Filter residuals in Figure 11 and the statistics in Table 5 indicate that the overall Trimble data quality (during this very short period of time) is similar to that of the Algonquin Park IGS station.
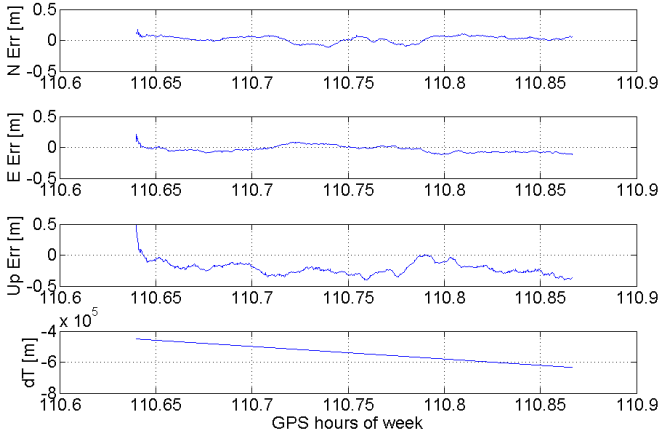

Figure 10: Position component differences and receiver clock errors of the Trimble antenna from the kinematic experiment.
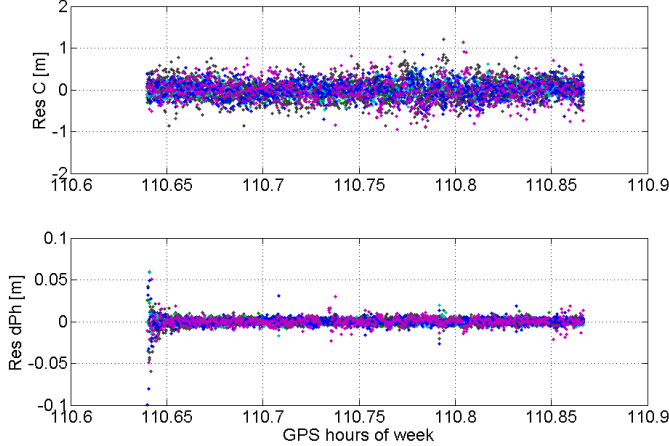

Figure 11: Filter residuals from of the Trimble data processing from the kinematic experiment. Top: pseudoranges. Bottom: carrier-phase differences.

Position Error Components [cm]			
	North	East	Up
Mean	1.0	-4.0	-23.0
Std. Dev.	10.0	7.0	16.0
r.m.s.	10.0	8.0	28.0
Measurement Residual r.m.s. [cm]			
Code	21.0	dPhase	1.0

Table 5: Trimble kinematic data processing statistics ignoring the initial 20 epochs of data.

Sampling Interval Testing

The relationship between the sampling rate and quality of the positioning results was studied as a part of the point positioning filter development. Table 6 shows the mean and the standard deviation of position components of the UNB Gillin Hall Garmin data processing with different data sampling rates. A 1-second dataset was collected and down-sampled to yield the desired sampling rates.

Sampling Interval [s]		1	5	10	30
North Error	Mean [cm]	78	78	74	72
	Std.Dev. [cm]	116	71	58	29
East Error	Mean [cm]	21	19	14	17
	Std.Dev. [cm]	88	55	44	24
Up Error	Mean [cm]	-71	-59	-60	-56
	Std.Dev. [cm]	280	196	164	85

Table 6: Sampling intervals and position error means and standard deviations for static Garmin data from UNB Gillin Hall. Note that the point-positioning processor used different settings than in the previous tests.

The results in Table 6 indicate that with longer sampling intervals, there is a decrease in standard deviations but the position component biases remain on the same level. This could be explained by the second hypermatrix in Equation (2), which includes multiplications of the t and t-1 epoch geometry matrices (A_{t-1} and A_t). The matrix multiplication indicates that the more significant between-epoch geometry change, which occurs, the more useful the delta-phase measurements, and subsequently the "smoother" the resulting estimate. In conclusions, the filter convergence time is similar using high and low sampling interval.

Comparison of Single-Frequency and Ionosphere-Free Results

A comparison of single-frequency and ionosphere-free results from the Algonquin Park station from a 24-hour dataset on 26 September 2004 was performed to confirm the accuracy of the final ionospheric maps from the IGS products table [IGS, 2005]. Two positioning solutions are plotted in Figure 13 for comparison.
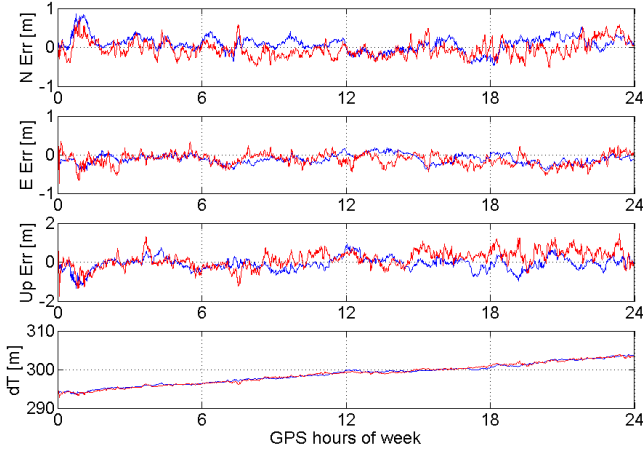
Figure 13: Single-frequency pseudorange (C1) and time-differenced carrier-phase positioning results (blue) and ionosphere-free pseudorange and ionosphere-free time-differenced carrier-phase positioning results (red) for a 24-hour Algonquin Park dataset.
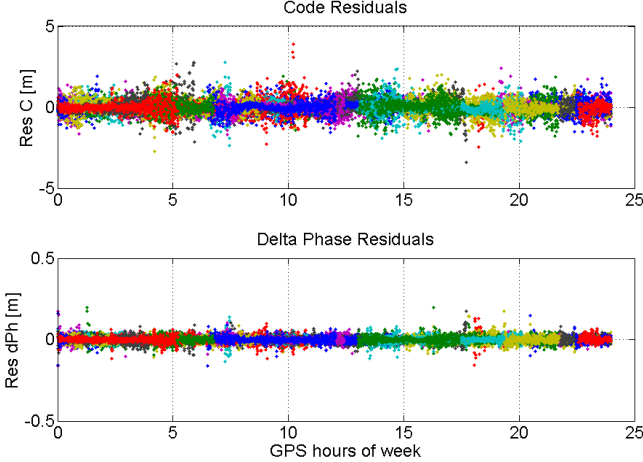

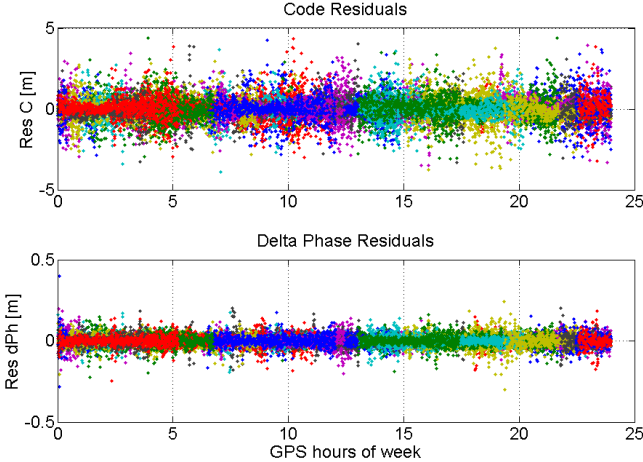Figure 14: Filter residuals from the single-frequency Algonquin Park data processing.

Figure 15: Filter residuals from the ionosphere-free Algonquin Park data processing.

Position Error Components [cm]			
	North	East	Up
Mean	5.0 *–4.0*	-9.0 *-13.0*	-3.0 *18.0*
Std. Dev.	21.0 *20.0*	13.0 *21.0*	30.0 *42.0*
r.m.s.	22.0 *21.0*	15.0 *21.0*	30.0 *45.0*
Measurement Residual r.m.s. [cm]			
Code	40.0 *68.0*	dPhase	2.0 *3.0*

Table 7: Single-frequency and *ionosphere-free* (italics) data processing statistics for a 24-hour Algonquin Park dataset ignoring the initial 20 epochs of data.

Single-frequency and ionosphere-free data processing statistics for a 24-hour Algonquin Park dataset in Table 7 show that there is no significant bias in the up component if the ionosphere-free measurements are used. The reason for an 18 cm up component bias for the ionosphere-free results remains to be investigated. Up-component standard deviation is bigger than the horizontal component standard deviations for both sets of results because of the absence of solid Earth tides and ocean tide loading models, residual tropospheric delay estimation, antenna phase center variation, carrier-phase wind up correction model, and due to satellite geometry limitations. Overall the position components standard deviations and the measurement residual r.m.s. of the ionosphere-free solutions are bigger than those of the single-frequency solution because of the factor-two higher noise in the ionosphere-free measurement linear combinations.

DISCUSSION

Before summarizing and commenting on the results, it is worth commenting on the impact of the individual error sources:

Ionosphere – The IGS atmospheric products table includes the accuracy of the rapid and final ionospheric TEC grid maps of 2-9 and 2-8 TECU, respectively [IGS Products Table, 2005]. 1 TECU corresponds to 16 cm on L1. Experimental comparison of single-frequency and ionosphere-free positioning results (Table 7) shows that there is no significant bias in the up component of the single-frequency results. Closer examination of the pseudorange residuals from both solutions (Figure 14 and Figure 15) reveals certain structures in the single-frequency ones, which are caused by residual ionospheric delay errors.

IGS orbits and clocks – When single and dual-frequency results are computed, one has to pay attention to the IGS orbits and clock products compatibility issues, namely P1-C1 biases and satellite and receiver differential code delays (DCBs). The latter is also known as group delay (TGD) [ICD-GPS-200C, 1999]. Some positioning result

differences were found, when orbit and clock products from different IGS processing centres were used. One reason for the existence of these differences is the use of different reference clocks at different IGS processing centres. To avoid this problem, all the results presented in this paper were generated using combined IGS products.

Troposphere - The hydrostatic component of the zenith delay can be modelled with millimetre accuracy (if accurate surface pressure measurements are available), but the water vapour component of the tropospheric delay provides a limiting factor. The expected residual zenith delay error after applying a model such as UNB3 would be typically at the few centimeter level [Collins, 1999]. It will be possible to estimate this error from the GPS data itself only if a long period of continuous carrier-phase observations is available. The residual tropospheric delay estimation was not included in the solutions presented here, due to its small magnitude and the accuracy of single-frequency results and the difficulties in distinguishing between the ionospheric and tropospheric delay errors for low-elevation-angle observations.

Multipath – Figure 16 shows the presence of GPS signal reflections indicated by multipath fringes between hours 48 and 50. Multipath is present for more than half of this dataset. Even though the code observation noise was set to 10 m in the measurement covariance matrix and some large outliers were rejected in the code outlier detection process (see above), the positioning results are still worse than the results obtained from low-multipath observations. This experience indicates that multipath errors could be the limiting factor for low-cost receiver point positioning.
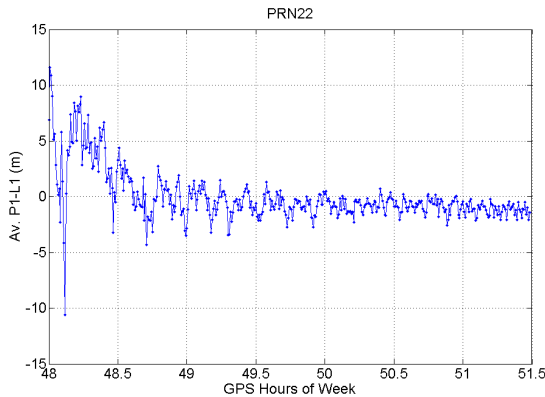

Figure 16: Averaged code minus phase observations for PRN 22 generated from the UNB Gillin Hall dataset.

Cycle slips – The functionality of the delta-phase residual outlier detection algorithm was verified by the analysis of the code minus phase observable. It is important to keep in mind that residual outlier detection is reliable only if the stochastic modeling is correct. The ratio of pseudorange to carrier-phase measurement accuracy

should reflect the actual receiver performance and the a-priori noise values should be close to the actual values.

Station	North Error r.m.s.	East Error r.m.s.	Up Error r.m.s.	Code Res. r.m.s.	dPh. Res. r.m.s.
Algonquin	13.0	8.0	27.0	30.0	3.0
Gillin Hall	61.0	56.0	110.0	157.0	6.0
Head Hall	41.0	4.0	24.0	81.0	7.0

Table 8: Static positioning results summary. All results are in centimetres.

Table 8 summarizes the results of the static positioning experiments. The 3.5-hour Algonquin Park dataset of 22 February 2005 shows a 2 decimetre up component r.m.s. error. The 24-hour dataset from the same station recorded on 26 September 2004 (Table 7) shows a 3 decimetre up component r.m.s. error. These results are encouraging, but they are achievable only with geodetic-quality GPS receivers. A low-quality GPS receiver in a multipath-rich environment achieved only 8 dm up component error r.m.s., but the results are significantly better (2 dm up component r.m.s.) when a lower multipath location was used. There are still some issues with the UNB Head Hall dataset (e.g., north component bias in Table 3), which will be investigated.

Dataset	North Error r.m.s.	East Error r.m.s.	Up Error r.m.s.	Code Residual r.m.s	dPhase Residual r.m.s.
Garmin	103.0	35.0	141.0	151.0	2.0
Trimble	10.0	8.0	28.0	22.0	1.0

Table 9: Kinematic positioning results summary. All results are in centimetres.

Table 9 summarizes the results of the kinematic data processing. The results presented in this table are based on a considerably shorter observation time period than those of static positioning. The high-quality receiver data from a moving receiver are almost as good as those of a high-quality static receiver. Results of the Garmin receiver data processing are about two times worse than those of the multipath-contaminated static site.

During the kinematic experiment, the Garmin receiver encountered difficulties with GPS signal tracking for both pseudorange and carrier-phase measurements. Presence of pseudorange outliers makes one question the reliability of the PC data recording software. For the high-quality receivers, the kinematic positioning results are similar to

the static ones and it was expected that the low-cost receivers would behave in the same way.

The overall conclusion is that the results of the low-cost GPS receiver point positioning depend on the receiver tracking capabilities, i.e. hardware-based-limit, and on the handling of measurement errors. If the atmospheric biases are properly accounted for, multipath is the limiting factor. The technique works for static and kinematic applications. About 50 cm 3D error r.m.s. is achievable.

FUTURE RESEARCH

The first recommendation for future research is to repeat the static and kinematic data collection with a Garmin OEM receiver, which outputs the pseudorange and carrier phase data by design and in a published format.

Quality control issues, or the reliability of the outlier detection algorithm, is mentioned for future work because cycle slip detection is highly dependent on the a priori information of the receiver data quality. To obtain this information, a code-only pre-processing step could be performed. For the future development of this point positioning filter, it would be desirable to develop a phase-only cycle-slip detection algorithm to identify and reject the corrupted measurements before processing.

Residual ionospheric delay estimation could improve the positioning results. A second approach that is already being investigated is the use of a 3-dimensional ionospheric model. One version of our point positioning software is capable of obtaining and using data from a global 3D ionospheric model instead of 2D global ionospheric maps. In order to validate the performance of the 3D model, we intend to process data reflecting different ionospheric conditions (different sites and different days).

It was mentioned earlier that multipath errors could be the limiting factor for low-cost receiver positioning. Since multipath, atmospheric delays, and higher-noise observations affect the measurements primarily from low-elevation angle satellites, we created an experimental implementation of exponential elevation-angle weighting [Jin, 1996]. So far, we do not see any improvements when this algorithm is used, but it is considered as a future research topic.

Real-time implementation of the point-positioning software developed at UNB would be relatively simple. Once the interface with the real-time orbit, clock and ionospheric corrections is built, the software will be ready for real-time processing. The processor currently does not include any pre-processing or backward smoothing. The exponential elevation angle weighting, which requires the residuals, is not essential.

REFERENCES

Beran, T., D. Kim, and R.B. Langley (2003). "High-Precision Single-Frequency GPS Point Positioning" *Proceedings of the 16th International Technical Meeting of the Satellite Division of The Institute of Navigation*, Portland, Oregon, U.S.A., 9-12 September 2003; The Institute of Navigation, Alexandria, Virginia, U.S.A.; pp. 1192-1200.

Beran, T., S. B. Bisnath, and R.B. Langley (2004). "Evaluation of High-Precision Single-Frequency GPS Point Positioning Models", *Proceedings of the 17th International Technical Meeting of the Satellite Division of The Institute of Navigation*, Long Beach, California, U.S.A., 21-24 September 2004; The Institute of Navigation, Alexandria, Virginia, U.S.A; pp. 1892-1901.

Bisnath, S.B. and R.B. Langley (2002). "High-Precision, Kinematic Positioning with a Single GPS Receiver." *Navigation: Journal of the Institute of Navigation*, Vol. 49, No. 3, Fall 2002; The Institute of Navigation, Alexandria, Virginia, U.S.A.; pp. 161-169.

Bisnath, S.B. (2004). *Precise Orbit Determination of Low Earth Orbiters with a Single GPS Receiver-Based, Geometric Strategy.* Ph.D. Dissertation, Department of Geodesy and Geomatics Engineering Technical Report No. 220, University of New Brunswick, Canada, 143 pp.

Boudreau, B. (1993). *GPS Multipath Detection with Varying Antenna Height.* B.Sc.E. Report, Department of Geodesy and Geomatics Engineering, University of New Brunswick, Canada, 27 pp.

Collins, J.P. (1999). *Assessment and Development of the Tropospheric Delay Model for Aircraft Users of the Global Positioning System*. M.Sc.E. Thesis, Department of Geodesy and Geomatics Engineering Technical Report No. 203, University of New Brunswick, Canada, 174 pp.

ICD-GPS-200C(1999). *Navstar GPS Space Segment/Navigation User Interface Control Document*. ARINC Research Corporation, El Segundo, California, U.S.A., 138 pp.

International GNSS Service (IGS) (2005). "IGS Products Table." IGS. [On-line] 8 July, 2005. http://igscb.jpl.nasa.gov/components/prods.html

Jin, X. (1996). *Theory of Carrier Adjusted DGPS Positioning Approach and Some Experimental Results.* Delft University Press, Delft, The Netherlands, 162 pp.

Kouba, J. and P. Héroux (2001). "Precise Point Positioning Using IGS Orbit and Clock Products." *GPS Solutions*, Vol. 5, No. 2, pp.12-28.

Misra, P. and P. Enge (2001) *Global Positioning System: Signals, Measurements, and Performance.* Ganga-Januma Press, Lincoln, Massachusetts, 390 pp.

Muellerschoen, R., B. Iijima, R. Meyer, Y. Bar-Sever, and E. Accad (2004). "Real-Time Point Positioning Performance Evaluation of Single-Frequency Receivers Using NASA's Global Differential GPS System." *Proceedings of the 17th International Technical Meeting of the Satellite Division of The Institute of Navigation*, Portland, Oregon, U.S.A., 21-24 September 2004; The Institute of Navigation, Alexandria, Virginia, U.S.A.; pp. 1872-1880.

Schaer, S., W. Guntner, and J.Feltens (1998). "IONEX: The IONosphere Map Exchange Format Version 1." *Proceedings of the IGS AC Workshop*, Darmstadt, Germany, 9-11 February, 1998, ESA/ESOC, Darmstadt, Germany, pp. 233-237.

Tétreault, P., J. Kouba, P. Héroux, and P. Legree (2005). "CSRS-PPP: An Internet Service for GPS User Access to the Canadian Spatial Reference Frame." *Geomatica*, Vol. 59, No. 1, pp. 17-28.